Research and Design of Coordinated Control Strategy for Smart Electromechanical Actuator System

HAO Zhenyang, ZHANG Qiyao, CHEN Huajie, CAO Xin, MIAO Wei*

College of Automation Engineering, Nanjing University of Aeronautics and Astronautics, Nanjing 211106, P. R. China

(Received 21 April 2022; revised 11 May 2022; accepted 21 August 2022)

Abstract: In order to improve the frequency response and anti-interference characteristics of the smart electromechanical actuator (EMA) system, and aiming at the force fighting problem when multiple actuators work synchronously, a multi input multi output (MIMO) position difference cross coupling control coordinated strategy based on double-closed-loop load feedforward control is proposed and designed. In this strategy, the singular value method of return difference matrix is used to design the parameter range that meets the requirements of system stability margin, and the sensitivity function and the H_∞ norm theory are used to design and determine the optimal solution in the obtained parameter stability region, so that the multi actuator system has excellent synchronization, stability and anti-interference. At the same time, the mathematical model of the integrated smart EMA system is established. According to the requirements of point-to-point control, the controller of double-loop control and load feedforward compensation is determined and designed to improve the frequency response and anti-interference ability of single actuator. Finally, the 270 V high-voltage smart EMA system experimental platform is built, and the frequency response, load feedforward compensation and coordinated control experiments are carried out to verify the correctness of the position difference cross coupling control strategy and the rationality of the parameter design, so that the system can reach the servo control indexes of bandwidth 6 Hz, the maximum output force 20 000 N and the synchronization error $\leqslant$0.1 mm, which effectively solves the problem of force fighting.

Key words: smart electromechanical actuator (EMA); force fighting; coordinated control strategy; cross coupling control; singular value method of return difference matrix; sensitivity H_∞ norm control

CLC number: V11 **Document code:** A **Article ID:** 1005-1120(2022)05-0507-14

0 Introduction

Under the background of aircraft electrification, the wide use of electric actuator system has become a trend[1]. Smart electromechanical actuator (EMA) is a relatively new actuator concept in more electric and all electric aircraft. It has great development potential and is expected to be applied to key electric transmission systems such as aircraft braking, rudder surface control and oil pump in the future[2-3]. Smart EMA integrates the motor, controller and transmission unit, and is connected with the aircraft controller through the data line, which improves the reliability, maintainability and servo tracking characteristics of the whole flight control system[4].

Since the 1970s, the first development in the field of space applications has stimulated the development of EMAs. Smart EMAs with high power density and high control performance are one of the key equipments of airborne electromechanical systems, and have been applied in the flight control systems of aviation F-18, F-35, C-130, space shuttle, crew return aircraft X-38 and unmanned aerial vehicle[5-6]. The Chinese Academy of Aerospace has also carried out in-depth research on the actuation technology of smart EMAs. However, it is still in the initial stage of development compared with for-

*Corresponding author, E-mail address: zhangqiyao@nuaa.edu.cn.

How to cite this article: HAO Zhenyang, ZHANG Qiyao, CHEN Huajie, et al. Research and design of coordinated control strategy for smart electromechanical actuator system[J]. Transactions of Nanjing University of Aeronautics and Astronautics, 2022, 39(5): 507-520.

http://dx.doi.org/10.16356/j.1005-1120.2022.05.001

eign technologies[7-8], especially in the development of high-voltage smart EMA system with high reliability, high frequency response, high integration and high thrust. The reliability, stability and control characteristics of actuator products need to be improved.

Compared with ordinary EMAs, smart EMAs have more excellent servo tracking characteristics and anti-interference ability, and their performance requirements such as high frequency response and low tracking error put forward higher requirements for control algorithms[3]. On the basis that the control strategy meets the servo performance requirements, the smart EMA system also needs to have the ability to output large load thrust, at the same time have high reliability and strong fault tolerance. Therefore, multiple smart EMAs are often used to drive the load surface together. However, due to component errors and installation deviations, the drive of multiple smart EMAs cannot be completely synchronized, which inevitably leads to force fighting among multiple actuators[9-10].

At present, researchers in various countries have carried out some studies on the issue of force fighting. Ref.[11] points out that whether it is an actuator system with similar redundancy configuration or a hybrid actuator system with dissimilar redundancy, the force equalization control strategy is the best choice to reduce the force fighting. Refs.[11-12] list several typical force equalization algorithms, the main idea of which is to reduce the force fighting by reducing the displacement deviation or force deviation of the two-channel output by means of compensation. Refs.[13-15] carried out modelling for the hybrid actuation system, and used the integral controller of position feedback and force feedback to deal with the force fighting. It was concluded that position feedback can restrain the force fighting more effectively than force feedback. Therefore, in order to obtain a balanced actuating output force, it is necessary and critical to study a high-performance multi motor position coordinated control strategy and realize its application in engineering.

Take dual motor control as an example, the coordinated control mainly includes parallel control, master-slave control, and cross coupling control[16]. Both the parallel control and the master-slave control belong to the non-coupling control, and are only suitable for occasions with low requirements for synchronization. The cross coupling control strategy of dual motor was proposed by Koren in 1980[17], adding error feedback on the basis of parallel control to improve the system synchronization and anti-interference ability. However, since the purpose of coordinated control is to make the position or rotational speed of the two motors exactly the same or to maintain a certain proportion, the system only contains one input and does not belong to a multiple input multiple output (MIMO) system. There are difficulties and limitations in the design of synchronization parameters, which is not conducive to the practical application of engineering.

Firstly, aiming at the high-frequency response and "point-to-point" control requirements of the smart EMA system, this paper adopts the position-current loop double-loop control method for a single actuator, and designs the PID parameters of the loop regulators. In addition, a load feedforward control strategy is introduced to reduce the negative impact of random load disturbance of the system. Secondly, in order to realize the large thrust output requirements, an innovative position difference cross coupling control strategy is proposed and designed through an MIMO system analysis method. The singular value method of return difference matrix is used to determine the parameter range of the regulator of position loop and position difference loop under the desired stability margin, and the optimal value of the parameters is selected in combination with the sensitivity H_∞ norm control theory, so as to ensure the dynamic, steady-state performance and anti-interference performance of the dual smart EMA system. Finally, experiments are carried out on the smart EMA experimental platform to verify the feasibility of the proposed control strategy and the rationality of parameter tuning. The experimental results show that the system achieves the specified servo performance index, and effectively solves the force fighting problem caused by the parallel driving of multiple smart EMAs.

1 Model and Control Strategy of Smart EMA System

In order to meet the requirements of high reliability, high safety and miniaturized actuation system of future aircraft, a highly integrated smart EMA system is designed to drive the rudder surface load, integrating the drive controller, motor, reducer and transmission mechanism, as shown in Fig.1. Among them, the permanent magnet synchronous motor (PMSM), reducer and ball screw are in series structure forming an electric actuator. The middle part is the mechanical transmission unit of the electric actuator, and two drive controllers are arranged on both sides. The two drive controllers adopt high thermal conductivity and high strength materials to connect with the housing where the actuating motors are located.

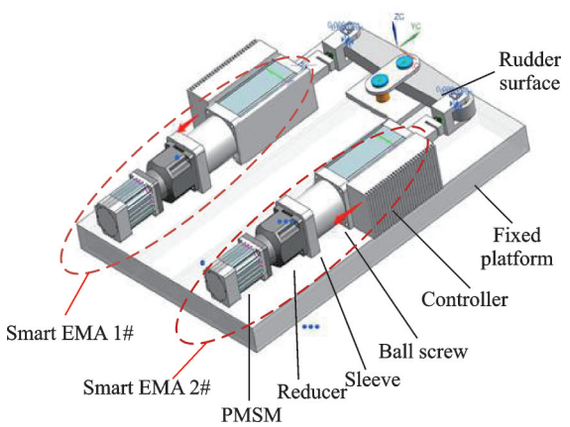

Fig.1 Integrated smart EMA system

As the power source of the system, the PMSM drives the reducer to rotate, and the shaft end of the reducer is connected to the ball screw, so as to drive the screw to extend or retract to realize the reciprocating linear operation of the load, thereby pushing the rudder surface to the specified angle or position.

1.1 Establishment of mathematical model

This section establishes the models of relevant components of the designed smart EMA system respectively. The single actuator is reasonably simplified, and the structure shown in Fig.2 is obtained. In Fig.2, T_{em}, θ_q, J_q and B_q are the output electromagnetic torque, rotation angle, moment of inertia and viscosity coefficient of the PMSM, respectively. J_{g1} and J_{g2} are the moments of inertia of the front and rear gears, and N is the reduction ratio. J_h and B_h are the moment of inertia and viscous coefficient on the ball screw side. θ_h and y are the output angle and linear displacement of the actuator, F_a is the axial thrust of the screw, and T_{eh} is the equivalent torque.

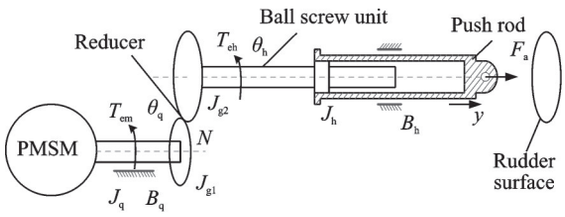

Fig.2 Simplified structure diagram of electric actuator

1.1.1 Model of ball screw

Assuming that the force of the ball screw on the rudder surface is F_a, the equivalent torque T_{eh} and moment of inertia J_{g3} on the ball screw shaft are as follows

$$T_{eh}=\frac{F_a\cdot \mathrm{Ph}}{2\pi\eta} \tag{1}$$

$$J_{g3}=m\left(\frac{\mathrm{Ph}}{2\pi}\right)^2 \tag{2}$$

where Ph is the lead of the ball screw, that is, the displacement of the linear motion of the ball screw corresponding to each revolution of the reducer. η is the efficiency of the ball screw traveling process, which is taken as 1 here.

The relationship between the actuator output angle θ_h and the linear displacement y is

$$\theta_h=\frac{2\pi}{\mathrm{Ph}}y \tag{3}$$

1.1.2 Model of reducer

The differential equations on both sides of the reducer are as follows

$$J_q\frac{\mathrm{d}^2\theta_q}{\mathrm{d}t^2}=T_{em}-B_q\frac{\mathrm{d}\theta_q}{\mathrm{d}t}-T_{eq} \tag{4}$$

$$(J_{g2}+J_h+J_{g3})\frac{\mathrm{d}^2\theta_h}{\mathrm{d}t^2}=T_{eh}-B_h\frac{\mathrm{d}\theta_h}{\mathrm{d}t}-T_h \tag{5}$$

where T_{eq} is the gear torques on the primary side, with $T_{eq}=T_{eh}/N$. Let

$$J_e=J_q+\frac{1}{N^2}(J_{g2}+J_h+J_{g3}) \tag{6}$$

$$B_e=B_q+\frac{1}{N^2}B_h \tag{7}$$

Then, the mathematical model of the mechanical part of the actuator is obtained as follows[18]

$$\begin{cases} T_{eq} - \dfrac{F_a \cdot \mathrm{Ph}}{2\pi N \eta} = (J_e s + B_e)\dfrac{\mathrm{d}\theta_q}{\mathrm{d}t} \\ y = \dfrac{\mathrm{Ph}}{2\pi N}\theta_q \end{cases} \tag{8}$$

1.1.3 Model of PMSM

Considering that the practical PMSM model is relatively complex nonlinear and strongly coupled, in order to facilitate the design and analysis of the system, a PMSM mathematical model is established through the dq coordinate transformation[18-19]. Using the vector control method with $i_d = 0$, the stator voltage equation is obtained, shown as

$$\begin{cases} u_d = -\omega_e L_q i_q \\ u_q = R_s i_q + p L_q i_q + \omega_e \psi_m \end{cases} \tag{9}$$

where R_s is the armature phase resistance of the motor, ω_e the electrical angular velocity of the rotor, and ψ_m the rotor flux linkage. u_q, i_q, L_q are the quadrature axis (q-axis) components of the stator voltage, current, and phase inductance, respectively.

The electromagnetic torque equation of PMSM is

$$T_{em} = \frac{3}{2} p_n \psi_m i_q \tag{10}$$

where p_n is the number of pole pairs of the motor.

1.2 Determination of control strategy

1.2.1 High frequency response servo control strategy

In PMSM servo control system, the position-speed-current three-loop control strategy is usually adopted. Smart EMA servo system belongs to fixed-point position tracking control, which has low requirements for speed accuracy control. In order to pursue better position dynamic response performance, realize the requirements of "point-to-point" position tracking and high frequency response, the speed loop of traditional three-loop control is removed and the double-closed-loop control strategy of position outer loop and current inner loop is adopted[18].

While improving the response speed of the smart EMA system, the amount of overshoot will also increase. In addition, when the load force increases, the negative impact of random load disturbance on the system control will gradually become prominent. Therefore, on the basis of double-loop control, a load torque observer is designed, and load feedforward control is used to optimize the control of the smart EMA, which can suppress overshoot and enhance the anti-interference ability[20]. The control strategy block diagram is shown in Fig.3, where r^* is the reference position, r the output position, APR the automatic position regulator, ACR the automatic current regulator, dq the synchronous rotation coordinate system, abc the natural coordinate system, and $\alpha\beta$ the static coordinate system.

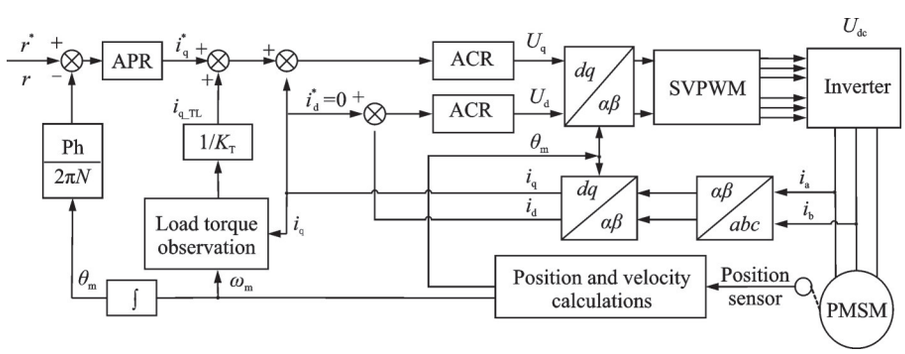

Fig.3 Structural block diagram of double-loop control system with load torque feedforward

1.2.2 Limitations of traditional synchronous loop control

After ensuring that the dynamic and steady state of a single smart EMA meets the performance index requirements, the coordinated control strategy of double-actuator drive motor is studied to adapt to the practical application scenario of large load thrust.

Parallel control is very easy to lose synchronization after being disturbed, resulting in serious force fighting[21]. Therefore, a position synchronous loop is usually added to the control loop, and the output

displacement of the two actuators is synchronized through the coordinated control of the synchronous loop, thereby reducing or even eliminating force fighting. The transfer function block diagram of the traditional synchronous loop control strategy is drawn, as shown in Fig.4.

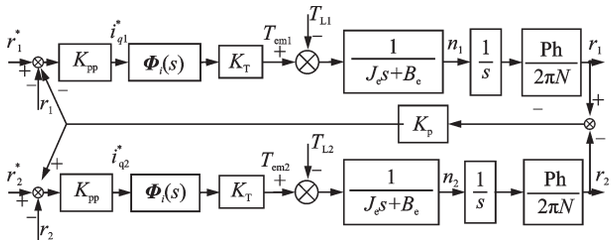

Fig.4 Transfer function block diagram of traditional synchronous loop control

In Fig.4, $\boldsymbol{\Phi}_i(s)$ is the current loop closed-loop transfer function, and K_{pp} and K_p are the proportional coefficients of the position loop and the position synchronous loop regulator.

In order to control the same output displacement, the two actuators are given the same position command, that is, $r_1^*=r_2^*$. However, in the actual system, the motor and gear structure of the two actuators are asymmetrical, so even if the position is given the same, the actual position output must be different, and there is a position difference between the actuators. Through the introduction of the position synchronous loop, the position difference of the two actuators is amplified by the synchronous loop regulator and then output to the position loop to adjust the position control signal, thereby realizing the purpose of reducing the position difference.

According to the coordinated control principle of the synchronous loop, the traditional synchronous loop control strategy is essentially a single input multiple output (SIMO) system. If the transfer function model of the control system is established, the obtained transfer function matrix is a non-square matrix with unequal number of rows and columns, and the stability and robustness analysis theories of general MIMO systems are not applicable to such systems. Therefore, although the traditional synchronous loop coordinated control strategy can reduce the position difference to a certain extent, it is very difficult to quantitatively design the synchronous loop parameters, which has limitations.

1.2.3 Position difference cross coupling control strategy

Since the synchronous loop coefficient will greatly affect the synchronization of the position output, it is necessary to break through the limitations of the traditional synchronous loop coordinated control in the design of loop parameters. The core idea of synchronous loop coordinated control is to control the output position difference of two motors to be 0. In order to accurately control the position difference, the closed-loop control loop of position difference is introduced, and a new coordinated control method is obtained, that is, position difference cross coupling control strategy. Fig.5 is the control block diagram of the strategy, obviously it is a MIMO control system.

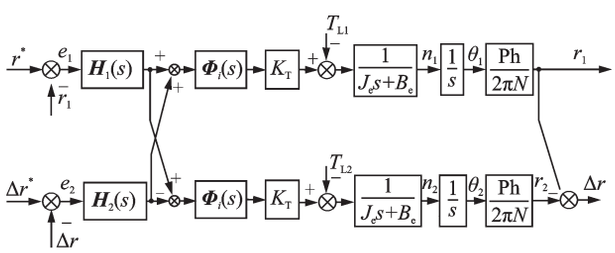

Fig.5 Transfer function block diagram of position difference cross coupling control

In Fig.5, $\boldsymbol{H}_1(s)$ is the position loop regulator, and $\boldsymbol{H}_2(s)$ the position difference loop regulator. The position difference cross coupling control strategy includes two inputs and outputs, and the parameter tuning of the loop regulator can be realized by applying the correlation analysis method of the MIMO system. The next section will carry out the specific design of the proposed control strategy.

2 Design of Control Strategy for Smart EMA System

The design focuses on the selected high-frequency response control strategy and the proposed position difference cross coupling control strategy. Table 1 lists the PMSM parameters of smart EMA system to guide the design of controller parameters.

Table 1 Parameters of PMSM

Parameter	Value
Operating voltage U_{dc}/V	270
Rated current I_{dc}/A	20
Rated speed n/(r•min^{-1})	7 500
Number of pole pairs p_n	5
d-axis inductance L_d/mH	2.12
q-axis inductance L_q/mH	2.11
Armature phase resistance R_m/Ω	0.22
Flux linkage ψ_m/Wb	0.128 7
Equivalent moment of inertia J_e/(kg•m^2)	1.38×10^{-3}
Equivalent viscosity coefficient B_e/[(N•m)•(rad•s^{-1})$^{-1}$]	7.44×10^{-3}

2.1 Parameter design of current inner loop

The servo performance of the smart EMA system is mainly determined by the performance of the current loop[22], so the design of the current loop is very important. The equivalent control structure of the current loop is shown in Fig.6, and the switching frequency f_{PWM} is taken as 10 kHz.

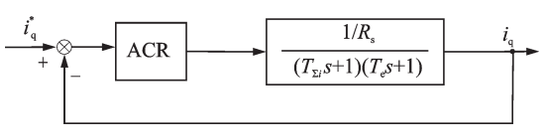

Fig.6 Equivalent control structure of current loop

In Fig.6, $T_{\Sigma i}=2T_{PWM}$, $T_e=L_s/R_s$ is the electromagnetic time constant of the motor. The current loop regulator ACR adopts PI control, K_{cp} is the proportional coefficient, and τ_{ci} is the integral time constant. Applying the zero-pole cancellation design method to eliminate the uncorrected dominant pole of the system is beneficial to improve the current loop frequency response. Let $\tau_{ci}=T_e$, the closed-loop transfer function is obtained as

$$\boldsymbol{\Phi}_i(s)=\frac{K_I}{T_{\Sigma i}s^2+s+K_I} \tag{11}$$

where $K_I=K_{cp}/(\tau_{ci}R_s)=K_{cp}/L_s$.

For the typical second-order system of Eq.(11), take $\xi=0.707$ to design the current loop parameters, and the obtained current loop regulator parameters are as follows

$$\begin{cases} K_{cp}\approx\dfrac{L_q}{6\xi^2T_{PWM}}=7.002 \\ K_{ci}=\dfrac{K_{cp}}{T_i}=\dfrac{R_s}{6\xi^2T_{PWM}}=733.5 \end{cases} \tag{12}$$

2.2 Design of load feedforward compensation strategy

The control system of the smart EMA is weak in dealing with random load disturbance. In order to improve the anti-interference of the system, load feedforward is used to compensate the current loop control. The addition of load feedforward will not affect the characteristics of current loop feedback control, which can greatly eliminate steady-state errors, improve the dynamic performance of the system, and reduce load disturbances, including low-frequency strong disturbances[22]. The schematic diagram of load feedforward compensation is shown in Fig.7.

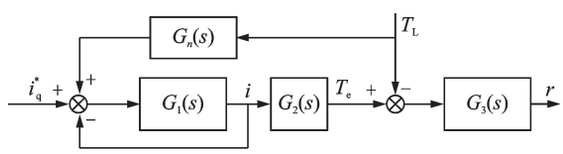

Fig.7 Schematic diagram of load torque feedforward

In order to observe the load situation synchronously, Luenberger load torque state observer is used for observation. Select ω_m and T_L as the state quantities, the closed-loop state space expression of the state observer is

$$\begin{cases} \dfrac{\mathrm{d}}{\mathrm{d}t}\begin{bmatrix}\hat{\omega}_m\\ \hat{T}_L\end{bmatrix}=\begin{bmatrix}-B/J & -1/J\\ 0 & 0\end{bmatrix}\begin{bmatrix}\hat{\omega}_m\\ \hat{T}_L\end{bmatrix}+ \\ \qquad\begin{bmatrix}K_t/J\\ 0\end{bmatrix}i_q-\boldsymbol{K}(\hat{y}-y) \\ \hat{y}=[1\quad 0]\begin{bmatrix}\hat{\omega}_m\\ \hat{T}_L\end{bmatrix} \end{cases} \tag{13}$$

where $\boldsymbol{K}=[k_1\ \ k_2]^T$ is the state feedback gain matrix, and the variable with superscript "^" the state variable corresponding to the system variable in the observer. Further derivation obtains the observer system matrix

$$\boldsymbol{F}=\begin{bmatrix}-B/J & -1/J\\ 0 & 0\end{bmatrix}-\begin{bmatrix}k_1\\ k_2\end{bmatrix}[1\quad 0]= \begin{bmatrix}-B/J-k_1 & -1/J\\ -k_2 & 0\end{bmatrix} \tag{14}$$

Combining with the knowledge of modern control principles[23], it can be known that the torque load observer is fully observable only when all the eigenvalues of the observer system matrix $\boldsymbol{F}$ have

negative real parts. Set the desired poles as α and β, and obtain the expression of the state feedback gain matrix $\boldsymbol{K}$ about α and β, shown as

$$\begin{cases} k_1 = -(\alpha+\beta) \\ k_2 = -\alpha\beta J \end{cases} \tag{15}$$

If the observation results of the designed load observer are feedforward compensated to the current loop, the impact of external load disturbance on the system can be effectively reduced[20].

2.3 Loop design of position difference cross coupling control strategy

After completing the design of the current loop with load torque feedforward compensation, according to the proposed position difference cross coupling control strategy, the system position loop and position difference loop controller parameters are tuned by using the stability margin and robustness analysis method of the MIMO system.

2.3.1 Stability margin of MIMO system

For multi-variable linear steady-state systems, the margin value of a single channel is generally used as an index to test the relative stability of the system in engineering, but it is not suitable to measure the situation when the gain and phase of each channel of the system change at the same time. The singular value method of system return difference matrix provides an idea to solve this problem[24]. The stability margin of the system is determined by calculating the minimum singular value of the return difference matrix, which has the advantage of small amount of calculation.

The stability margin represents the "distance" between the system and the critical stability. Therefore, the stability margin of the system can be evaluated by introducing a disturbance into the original system to make the system just reach the critical stable state[25]. For the general feedback system, as shown in Fig.8, where $\boldsymbol{G}(s)$ is the system open-loop transfer function matrix, the measurement matrix $\boldsymbol{L}(s)$ is introduced at the input and taken as the following diagonal form.

$$\boldsymbol{L}(s) = \mathrm{diag}\left\{k_i \exp(\mathrm{j}\phi_i)\right\} \quad i = 1,2,3,\cdots,n \tag{16}$$

When the system reaches critical stability, the maximum allowable value of the simultaneous change of gain k_i and phase ϕ_i in all loops is defined as the gain margin and phase margin of the system.

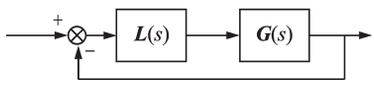

Fig.8 Unit negative feedback control system model

If the system remains stable after introducing the measurement matrix $\boldsymbol{L}(s)$, the system return difference matrix should meet the following requirements

$$\underline{\sigma}(\boldsymbol{I}+\boldsymbol{LG}) > 0 \tag{17}$$

where $\underline{\sigma}$ represents the minimum singular value of the matrix. The minimum singular value of the return difference matrix within the working frequency range of the system is the standard to measure the stability of the system. Since the actuator system without measurement matrix is stable and the return difference matrix $\boldsymbol{I}+\boldsymbol{G}$ is nonsingular, the separation characteristics of the matrix are used to separate $\boldsymbol{L}$ and $\boldsymbol{G}$ in the matrix $\boldsymbol{I}+\boldsymbol{LG}$, which is obtained as

$$\boldsymbol{I}+\boldsymbol{LG} = \left[(\boldsymbol{L}^{-1}-\boldsymbol{I})(\boldsymbol{I}+\boldsymbol{G})^{-1}+\boldsymbol{I}\right](\boldsymbol{I}+\boldsymbol{G})\boldsymbol{L} \tag{18}$$

The sufficient condition to make Eq.(18) hold is

$$\bar{\sigma}\left[(\boldsymbol{L}^{-1}-\boldsymbol{I})(\boldsymbol{I}+\boldsymbol{G})^{-1}\right] < 1 \tag{19}$$

According to the properties of singular value

$$\bar{\sigma}(\boldsymbol{A})\bar{\sigma}(\boldsymbol{B}) \geqslant \bar{\sigma}(\boldsymbol{AB}) \tag{20}$$

$$\bar{\sigma}(\boldsymbol{G}) = \frac{1}{\underline{\sigma}(\boldsymbol{G}^{-1})} \tag{21}$$

where $\bar{\sigma}$ represents the maximum singular value of the matrix. Analyzing Eq.(19) can obtain that

$$\bar{\sigma}(\boldsymbol{L}^{-1}-\boldsymbol{I}) < \underline{\sigma}(\boldsymbol{I}+\boldsymbol{G}) \tag{22}$$

Considering the simultaneous change of gain k_i and phase ϕ_i in each loop of the system, combined with Eq.(16), the sufficient conditions to ensure the stability of the system can be obtained as follows

$$\bar{\sigma}(\boldsymbol{L}^{-1}-\boldsymbol{I}) = \max_{i=1}^{n} \sqrt{\left(1-\frac{1}{k_i}\right)^2 + \frac{2}{k_i}(1-\cos\phi_i)} \leqslant \underline{\sigma}(\boldsymbol{I}+\boldsymbol{G}) \tag{23}$$

Since the actual system is known, $\underline{\sigma}(\boldsymbol{I}+\boldsymbol{G})$ can be calculated directly at any frequency. Taking the minimum singular value $\underline{\sigma}(\boldsymbol{I}+\boldsymbol{G})$ of the return difference matrix as the parameter, and assuming $\underline{\sigma}(\boldsymbol{I}+\boldsymbol{G}) \geqslant x$, according to Eq.(23), set gain $k_i=1$ and phase $\phi_i=0$ of each loop respectively, the gain margin (GM) and phase margin (PM) of the MI-

MO system can be obtained as

$$\mathrm{GM}=-20\lg(1-x),\ \mathrm{PM}=\arccos\left(1-\frac{x^2}{2}\right) \tag{24}$$

2.3.2 Loop parameter tuning based on stability margin

Based on the derived GM and PM above, the minimum singular value parameter range of the return difference matrix that meets the requirements of stability margin can be obtained. If the minimum singular value of the return difference matrix of the smart EMA system can be obtained and the relationship between the loop parameters and the minimum singular value can be established, the regulator parameters can be calculated reversely, so as to greatly simplify the tuning process of the regulator[26].

For the actuator system, considering the dynamic and steady-state performance of the system, its stability margin is usually taken as[23]

$$\mathrm{GM}=6.3\text{—}12.6\ \mathrm{dB},\ \mathrm{PM}=30^\circ\text{—}45^\circ \tag{25}$$

According to the singular value method of the return difference matrix, the minimum singular value range of the return difference matrix of the corresponding control system is directly calculated as

$$\underline{\sigma}\in[0.517\,8,0.765\,5] \tag{26}$$

Ideally, it is assumed that the parameters and structures of the electrical and mechanical components of the two smart EMAs are the same, and the load torque and disturbance are ignored. Pure proportional control is adopted for the position loop and position difference loop regulator, taking $\boldsymbol{H}_1(s)=\boldsymbol{H}_2(s)=K_\mathrm{p}$, and $\boldsymbol{\Phi}_i(s)=1$ to simplify the calculation. Take r_1 and r_2 as the open-loop output of the system, then write the open-loop transfer function matrix $\boldsymbol{G}(s)$ of the smart EMA system under the position difference cross coupling control (Fig.5) as follows

$$\boldsymbol{G}(s)=\begin{bmatrix}\dfrac{aK_\mathrm{p}}{s(J_\mathrm{e}s+B_\mathrm{e})} & \dfrac{aK_\mathrm{p}}{s(J_\mathrm{e}s+B_\mathrm{e})}\\ \dfrac{aK_\mathrm{p}}{s(J_\mathrm{e}s+B_\mathrm{e})} & -\dfrac{aK_\mathrm{p}}{s(J_\mathrm{e}s+B_\mathrm{e})}\end{bmatrix},\ a=K_\mathrm{T}\frac{\mathrm{Ph}}{2\pi N} \tag{27}$$

Calculate the return difference matrix $\boldsymbol{T}(s)$ as follows

$$\boldsymbol{T}(s)=\begin{bmatrix}\dfrac{aK_\mathrm{p}}{s(J_\mathrm{e}s+B_\mathrm{e})}+1 & \dfrac{aK_\mathrm{p}}{s(J_\mathrm{e}s+B_\mathrm{e})}\\ \dfrac{aK_\mathrm{p}}{s(J_\mathrm{e}s+B_\mathrm{e})} & -\dfrac{aK_\mathrm{p}}{s(J_\mathrm{e}s+B_\mathrm{e})}+1\end{bmatrix} \tag{28}$$

$\boldsymbol{T}(s)$ meets

$$\boldsymbol{T}(s)^\mathrm{H}\boldsymbol{T}(s)=\boldsymbol{T}(s)\boldsymbol{T}(s)^\mathrm{H} \tag{29}$$

Therefore, $\boldsymbol{T}(s)$ is a normal matrix whose singular value is equal to the modulus of the eigenvalue. The minimum singular value of the system return difference matrix under the position difference cross coupling control strategy is

$$\underline{\sigma}=\min\left|1+\frac{\sqrt{2}\cdot a\cdot K_\mathrm{p}}{s(J_\mathrm{e}s+B_\mathrm{e})}\right| \tag{30}$$

According to Eq.(30), the curve relationship between the minimum singular value of the system return difference matrix $\underline{\sigma}$ and the parameter K_p to be designed is shown in Fig.9.

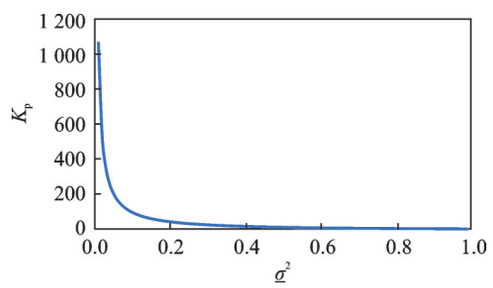

Fig.9 Relation between K_p and minimum singular value

As can be seen from Fig.9, the proportional regulator parameters of the position loop and the position difference loop are inversely proportional to the square of the minimum singular value. From the minimum singular value range of the system return difference matrix in Eq.(26), the range of the proportional coefficient K_p can be calculated inversely that

$$K_\mathrm{p}\in[6.43,27] \tag{31}$$

2.4 Analysis of anti-interference ability

When the smart EMA system works in practice, it will be subject to different types of external random disturbances, which will affect the stability of the system. Therefore, considering the anti-interference ability of the system, the parameter stability region is optimized based on the sensitivity H_∞ control theory to design a parameter that can not only

obtain the desired stability margin, but also have excellent anti-interference ability.

The sensitivity function matrix $\boldsymbol{S}(s)$ of MIMO system is the closed-loop transfer function matrix from interference $\boldsymbol{T}_{\mathrm{L}}$ to control error $\boldsymbol{e}$. Suppose the H_∞ norm of $\boldsymbol{S}$ is defined as

$$\|\boldsymbol{S}\|_\infty = \sup_{\omega\in\mathrm{R}^+} \bar{\sigma}\{\boldsymbol{S}(\mathrm{j}\omega)\} \tag{32}$$

According to the concept of operator induced norm[27], the norm of $\boldsymbol{S}$ is defined

$$\|\boldsymbol{S}\| = \sup_{x\neq 0} \frac{\|\boldsymbol{S}(\mathrm{j}\omega)\boldsymbol{x}\|_2}{\|\boldsymbol{x}\|_2} \tag{33}$$

When $\boldsymbol{S}\in H_\infty$, $\boldsymbol{x}\in L_2(-\infty,+\infty)$, there are the conclusions

$$\|\boldsymbol{S}\| = \sup_{x\neq 0} \frac{\|\boldsymbol{S}\boldsymbol{x}\|_2}{\|\boldsymbol{x}\|_2} = \sup_{\omega\in\mathrm{R}^+} \bar{\sigma}\{\boldsymbol{S}(\mathrm{j}\omega)\} = \|\boldsymbol{S}(\mathrm{j}\omega)\|_\infty \tag{34}$$

That is, the H_∞ norm is the induced norm of the second norm of the system in H_∞ space, which reflects the maximum gain of the signal from interference to control error. Therefore, the smaller the H_∞ norm of the system sensitivity function matrix $\boldsymbol{S}(s)$, the smaller the influence of external interference on the system control error.

According to the block diagram of position difference cross coupling control (Fig.5), the transfer function from interference $\boldsymbol{T}_{\mathrm{L}}$ to control error $\boldsymbol{e}$ can be obtained, and the sensitivity function matrix of two-dimensional smart EMA system can be established as

$$\begin{bmatrix} e_1 \\ e_2 \end{bmatrix} = \frac{b}{(J_{\mathrm{e}}s+B_{\mathrm{e}})s+bK_{\mathrm{T}}K_{\mathrm{p}}\boldsymbol{\Phi}_i(s)} \begin{bmatrix} 1 & 0 \\ 1 & -1 \end{bmatrix} \begin{bmatrix} T_{\mathrm{L1}} \\ T_{\mathrm{L2}} \end{bmatrix} = \boldsymbol{S}(s) \begin{bmatrix} T_{\mathrm{L1}} \\ T_{\mathrm{L2}} \end{bmatrix} \tag{35}$$

where $b=\mathrm{Ph}/2\pi N$, $\boldsymbol{\Phi}_i(s)=1/(2T_{\Sigma i}s+1)$. The closed-loop transfer function of the current loop is regarded as a first-order inertial link. The H_∞ norm of the sensitivity function of the smart EMA control system is calculated as

$$\|\boldsymbol{S}(s)\|_\infty = 1.618 \max_{\omega\in\mathrm{R}^+} \left| \frac{b}{(J_{\mathrm{e}}s+B_{\mathrm{e}})s+bK_{\mathrm{T}}K_{\mathrm{p}}\boldsymbol{\Phi}_i(s)} \right| \tag{36}$$

It can be seen from the above formula that the regulator parameter K_{p}, as one of the denominator terms, determines the value of the H_∞ norm of the system sensitivity function, and the two are negatively correlated. When K_{p} increases, theoretically $\|\boldsymbol{S}(s)\|_\infty$ decreases. Draw H_∞ norm curves of system sensitivity function under different K_{p} parameters in MATLAB, as shown in Fig.10.

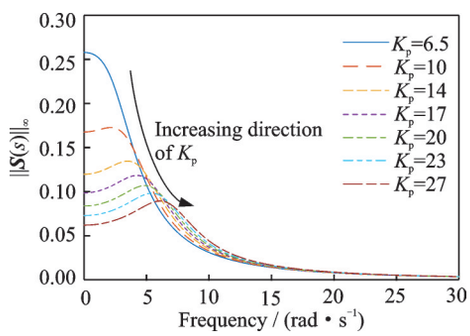

Fig.10 H_∞ norm curves of system sensitivity function under different K_{p} parameters

In Fig.10, the direction of the black arrow indicates the change trend of $\|\boldsymbol{S}(s)\|_\infty$ as the proportional coefficient K_{p} increases. It can be seen that with the increase of K_{p}, the H_∞ norm of the system sensitivity function decreases, which is consistent with the theoretical analysis.

When the H_∞ norm of the system sensitivity function is less than 1, it is considered that the system can maintain its stability under disturbance, and the smaller the value, the stronger the anti-interference ability. As can be seen from Fig.10, when K_{p} takes any value in the range of 6.43—27, the system can have excellent stability and anti-interference performance. When $K_{\mathrm{p}}=27$, the H_∞ norm of sensitivity function $\boldsymbol{S}(s)$ is the smallest, that is, the gain from interference to error is the smallest, and the anti-interference of the system is the strongest. Therefore, the optimal values of position difference and position difference loop regulator are obtained at $K_{\mathrm{p}}=27$.

3 Experimental Verification

3.1 Experimental platform

In order to verify the outstanding performance of the control strategy of the smart EMA system designed above, the system experimental platform is built and the corresponding experimental verification is carried out.

Fig.11 shows the physical picture of the experimental test platform. The test platform consists of

two smart EMAs with symmetrical structures, a simulated load platform and a rudder surface simulator. Among them, a single smart EMA integrates key components such as PMSM, controller, reducer and ball screw.

Fig.12 shows the hardware control structure of the smart EMA system, where SCI is the serial communication interface and CAN the controller area network. Smart EMA 1# and Smart EMA 2# have the same hardware structure and are both controlled by the host computer through SCI communication. Smart EMA 1# also acts as the main controller to deal with the coordination problem between the two actuators, and sends coordination commands to EMA 2# through CAN communication.

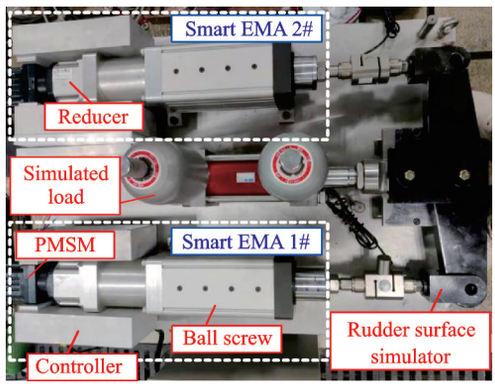

Fig.11 Experimental test platform

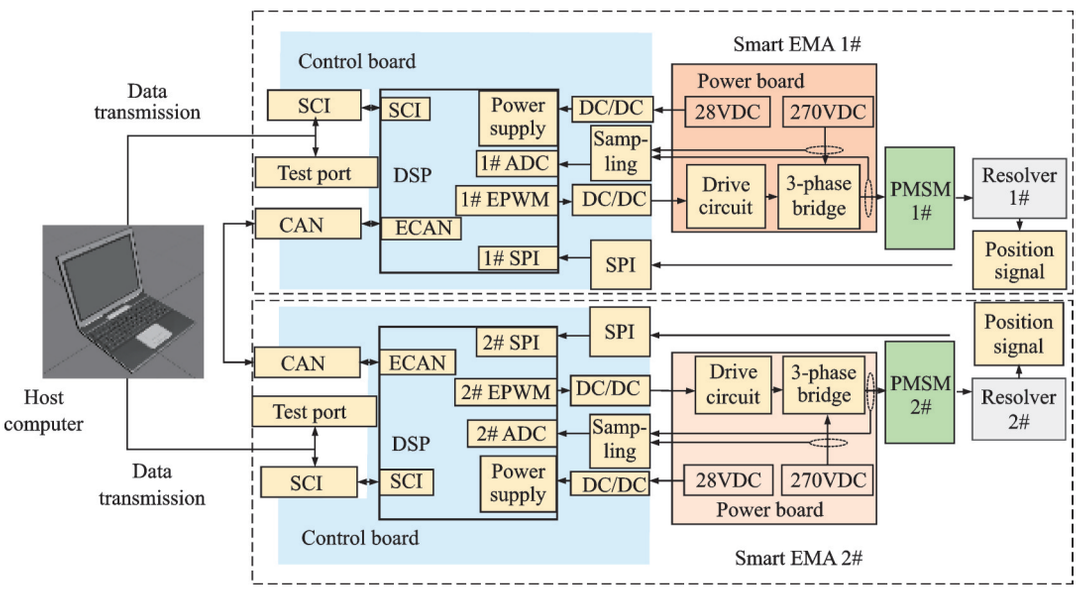

Fig.12 Structure diagram of system hardware control

Table 2 lists the performance requirements of the smart EMA system, and the corresponding performance indicators will be experimentally verified below.

Table 2 Performance index of smart EMA system

Parameter	Index
Operating voltage / V	270
Rated speed / ($m \cdot s^{-1}$)	$\geqslant$0.2
Synchronization error / mm	$\leqslant$0.1
Maximum output force / N	$\geqslant$20 000
Travel / mm	$\pm$10
20% travel bandwidth / Hz	$\geqslant$6

3.2 Frequency response experiment

It is generally believed that the amplitude attenuation is less than 0.707 times and the phase lag is less than 90°, the frequency response is good, and the output signal can track the input sinusoidal given signal well. Under no-load condition, the position-current double-loop control strategy is adopted, the given position signal amplitude is 2.5 mm, and the frequencies are 2, 4 and 6 Hz, respectively. The position frequency response waveform and i_q current waveform are observed, as shown in Fig.13.

Table 3 quantitatively analyzes the frequency response of the smart EMA system under different frequency given conditions. It can be seen from Table 3 that with the increase of the given frequency, the amplitude attenuation and phase lag of the actuator both increase. When the frequency is given as 6 Hz, the actuator can still maintain a better fre-

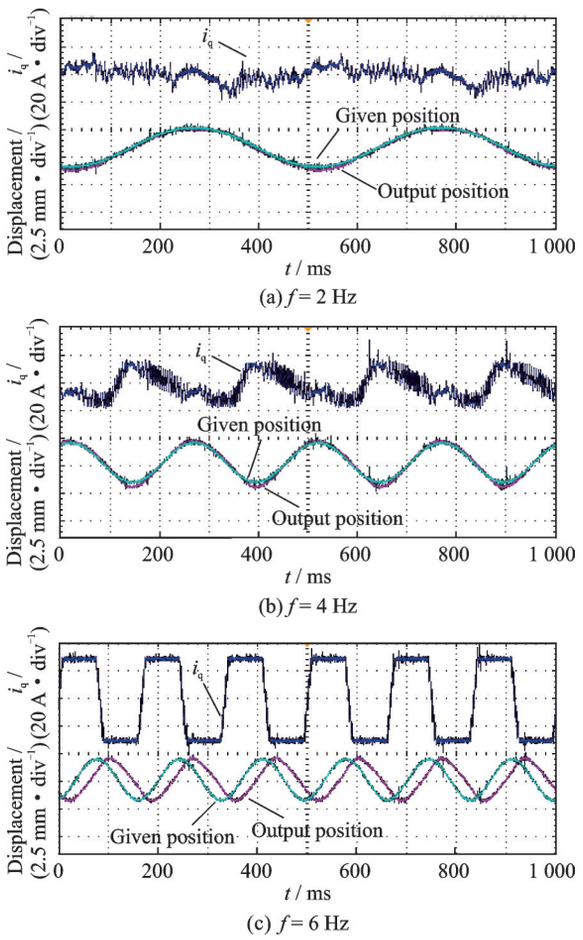

Fig.13 Experimental waveform of system frequency response under double-loop control

quency response, meeting the requirement of 20% travel bandwidth ⩾6 Hz. It can be known from the experimental results that the smart EMA has the servo response characteristics of high frequency response.

Table 3 Frequency response experimental data of smart EMA

Given frequency/ Hz	Amplitude attenuation/%	Phase lag/(°)
2	0.0	0.00
4	0.5	0.00
6	0.5	43.22

3.3 Load feedforward compensation experiment

Considering that the actuator disturbance will increase under heavy load, the application of load feedforward compensation based on double-loop control can effectively eliminate the load disturbance under heavy or full load.

When the load force is 20 000 N, the frequency response experimental results without and with load feedforward compensation are compared, as shown in Fig.14.

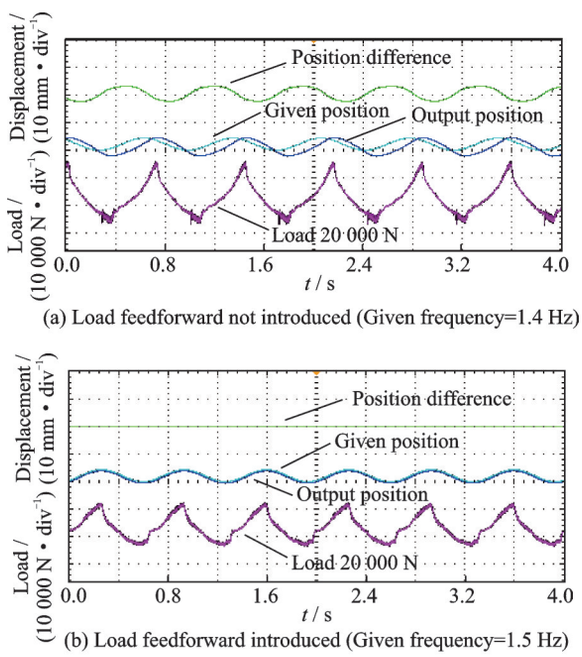

Fig.14 Frequency response experimental waveform comparison of load feedforward compensation

When the given position frequency reaches 1.4 Hz, the position waveform without load feedforward compensation has obvious phase lag, the lag angle exceeds 90°, and the signal tracking performance is poor. After the introduction of load feedforward compensation, the phase can still follow under the given frequency of 1.5 Hz, the position difference between the given and output is almost 0, and the frequency response is good. The experimental results show that the designed load feedforward compensation controller can effectively improve the position response bandwidth of the smart EMA system, make the system more suitable for heavy load conditions and enhance the anti-interference ability.

3.4 Coordinated control experiment of dual actuators

On the basis of ensuring that a single smart EMA has good dynamic and steady-state performance, the position difference cross coupling con-

trol strategy studied above is used to control the two actuators, and the comparative experiments of parallel control and cross coupling control of dual actuators are carried out.

When the load force is 5 000 N, the given position signal amplitude is 10 mm and the given frequency is 1.5 Hz, observe the position waveform and position difference waveform of dual actuators under the coordinated control of parallel control and position difference cross coupling, as shown in Fig.15.

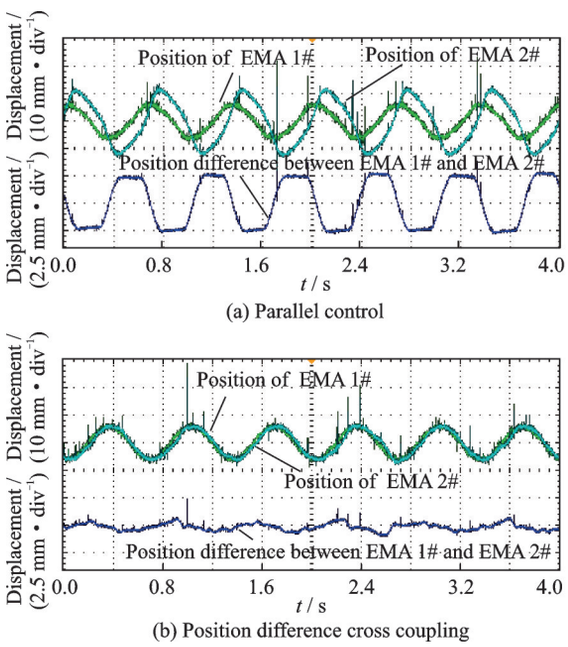

Fig.15 Frequency response experimental waveform of dual actuators under two different control strategies

It can be seen from Fig.15 that when the parallel control strategy is adopted, there is a large phase difference between the two actuators at the frequency of 1.5 Hz, which is about 60°. By contrast, the position difference cross coupling control strategy can maintain good coordination and consistency at the same given frequency, and the maximum position difference fluctuation is within 0.1 mm, which meets the requirement of the synchronization error of the smart EMA system $\leqslant$0.1 mm. Through the comparison of experimental results, it is concluded that compared with the parallel control, the proposed position difference cross coupling control strategy can effectively solve the problem of output position incoordination and force fighting of dual actuators, thereby improving the overall performance of the system.

4 Conclusions

According to the requirements of high frequency response, large load thrust and strong robustness of smart EMA system, this paper studies the position-current double-closed-loop control and load feedforward control strategy, and puts forward a position difference cross coupling control strategy based on MIMO system. The loop parameters are specifically designed to improve the motor servo characteristics and position output synchronization. The main work and conclusions of this paper include:

(1) The integrated smart EMA system is devised, and the mathematical models of ball screw, reducer and PMSM are established in turn. For a single smart EMA system, the strategy of position-current double-loop control combined with load feedforward compensation is adopted, and the loop control parameters are designed to ensure its dynamic, steady-state characteristics and anti-interference ability, so that the maximum output force and bandwidth meet the technical index requirements.

(2) The limitations of traditional synchronous loop control strategy in theoretical design are analyzed, and a coordinated control strategy based on position difference cross coupling is proposed. For the cross coupled position loop and position difference loop, the singular value method of MIMO system return difference matrix is utilized to determine the parameter stability range that meets the requirements of gain and phase margin, and then the optimization is carried out in the parameter stability region based on the sensitivity function. The parameter that make the system have excellent synchronization and robustness is finally determined.

(3) The experimental results show that the use of the position difference cross coupling control strategy can make the dual actuators maintain better coordination and consistency under the given signal of higher frequency, and alleviate the force fighting

between the actuators. Compared with the parallel control strategy, the coordinated control strategy proposed in this paper has certain advantages and can ensure that the smart EMA system meets the requirements of the synchronization error index. In conclusion, the designed control strategy of the smart EMA system has practical value for engineering application.

References

[1] SARLIOGLU B, MORRIS C T. More electric aircraft: Review, challenges, and opportunities for commercial transport aircraft[J]. IEEE Transactions on Transportation Electrification, 2015, 1(1): 54-64.

[2] SCHAEFER I, KAYSER A. Smart EMA: An approach to avoid unscheduled maintenance[C]//Proceedings of the AIAA 5th Aviation, Technology, Integration, and Operations Conference (ATIO). [S.l.]: AIAA, 2005, 2: 1108-1113.

[3] QIU X S. Research on the advanced actuators technology[J]. Aeronautical Science and Technology, 2009 (4): 6-8. (in Chinese)

[4] ZHU M J, XIA L Q, HU Y X, et al. Design of compact smart actuator[C]//Proceedings of 2017 IEEE Transportation Electrification Conference and Expo, Asia-Pacific (ITEC Asia-Pacific). [S.l.]: IEEE, 2017: 1-6.

[5] QIAO G, LIU G, SHI Z H, et al. A review of electromechanical actuators for more/all electric aircraft systems[J]. Journal of Mechanical Engineering Science, 2018, 232(22): 4128-4151.

[6] GUO H, XING W. Development of electromechanical actuators[J]. Acta Aeronautica et Astronautica Sinica, 2007, 28(3): 620-627. (in Chinese)

[7] HUANG M, HU X W, LI S J. Research on EMA servo control system[J]. Civil Aircraft Design & Research, 2019(4): 31-35. (in Chinese)

[8] LI F, ZHAO B Y. Design of intelligent electro-hydrostatic actuator[C]//Proceedings of the 2018 Military Equipment Technology Special Issue. Chongqing, China: [s.n.], 2018: 150-151, 154. (in Chinese)

[9] ZHOU Y J, ZHAO Y K, GE Y H. Fault tolerant control method and characteristic analysis of hydraulic redundant EMA system[J]. Journal of Beijing University of Aeronautics and Astronautics, 2008, 34(3): 285-289. (in Chinese)

[10] WANG C L, KANG R D. Force fighting analysis and mitigation algorithm design for redundant actuation system[C]//Proceedings of CSAA/IET International Conference on Aircraft Utility Systems (AUS 2020). [S.l.]: CSAA, 2020: 1142-1145.

[11] QI H T, TENG Y T. Force equalization control for dual-redundancy electro-hydrostatic actuator[J]. Journal of Beijing University of Aeronautics and Astronautics, 2017, 43(2): 270-276. (in Chinese)

[12] FU Y L, PANG Y, LIU H S, et al. Force fighting research of dual redundant hydraulic actuation system [C]//Proceedings of 2010 International Conference on Intelligent System Design and Engineering Application. Changsha, China: IEEE, 2010: 762-766.

[13] IJAZ S, YAN L, HAMAYUN M T. Fractional order modeling and control of dissimilar redundant actuating system used in large passenger aircraft[J]. Chinese Journal of Aeronautics, 2018, 31(5): 1141-1152.

[14] TIAN L, ZHANG Y S, WANG H W. Fly-by-wire actuation system modeling and force fight equalization research[J]. Journal of Northwestern Polytechnical University, 2020, 38(3): 643-648. (in Chinese)

[15] COCHOY O, HANKE S, CARL U B. Concepts for position and load control for hybrid actuation in primary flight controls[J]. Aerospace Science & Technology, 2007, 11(2/3): 194-201.

[16] WANG Y B, CAO K. Brief introduction of multi-motor synchronous control technology[J]. Small & Special Electrical Machines, 2019, 47(8): 69-73. (in Chinese)

[17] KOREN Y. Cross-coupled biaxial computer control for manufacturing systems[J]. Journal of Dynamic Systems, Measurement, and Control, 1980, 102(4): 265-272.

[18] CHEN W Z. The performance research on permanent magnet synchronous motor in EMA position servo system[D]. Nanjing: Nanjing University of Aeronautics and Astronautics, 2017: 8-20. (in Chinese)

[19] YUAN L. Modern PMSM control principle and MATLAB simulation[M]. Beijing: Beijing University of Aeronautics and Astronautics Press, 2016: 4-11. (in Chinese)

[20] HAN Z M. Research on control strategy of PMSM direct drive position servo system[D]. Nanjing: Nanjing University of Aeronautics and Astronautics, 2017. (in Chinese)

[21] HAO Z Y, WANG T, CAO X. Research on decoupling control strategy of position loop for vibration damping electric actuator[J]. Acta Aeronautica et Astronautica Sinica, 2021. DOI: 10.7527/S1000-6893.2021.25884. (in Chinese)

[22] SHAO C M. Research and design of active actuator system for active vibration absorption[D]. Nanjing: Nanjing University of Aeronautics and Astronautics, 2019. (in Chinese)

[23] HU S S. Automatic control principle[M]. Beijing: Science Press, 2007: 214-217. (in Chinese)

[24] WAMG Q G, YONG H, ZHEN Y, et al. On loop phase margins of multivariable control systems[J]. Journal of Process Control, 2008, 18(18): 202-211.

[25] ZHAI F C, SHI Z K, DAI G Z. Several definitions of MIMO system stability margin[J]. Flight Dynamics, 2002, 20(2): 6-9. (in Chinese)

[26] HAO Z Y, LI X, CAO X, et al. A cross-coupled control strategy of phase difference for electric vibration damping actuator[J]. IEEE Access, 2020, 8: 213887-213898.

[27] MAO S B. Aircraft robust controller design and visual simulation[D]. Xi'an: Northwestern Polytechnical University, 2005. (in Chinese)

Acknowledgements This work was supported by the National Natural Science Foundation of China (No.52077100) and the Aviation Science Foundation (No.201958052001).

Authors Prof. **HAO Zhenyang** received the B.S. degree in electrical engineering from Nanjing Normal University in 2004, and Ph.D. degree in power electronics and motion drive from Nanjing University of Aeronautics and Astronautics in 2010, respectively. From 2014 to 2015, he was a visiting scholar at the University of Wisconsin-Madison, USA. From 2010 to present, he has been engaged in the teaching and research with the Department of Electrical Engineering, College of Automation Engineering, Nanjing University of Aeronautics and Astronautics (NUAA). His current research interests include new energy power electronic conversion technology, aviation power supply and power actuator technology, electric vehicle motor design and driving technology.

Ms. **ZHANG Qiyao** is currently studying for a master's degree in electrical engineering in NUAA, China. Her main research direction is servo control and coordinated control of permanent magnet synchronous motor (PMSM).

Author contributions Prof. **HAO Zhenyang** contributed to the background of the study and designed the study. Ms. **ZHANG Qiyao** designed the control strategy, conducted the experiment and wrote the manuscript. Mr. **CHEN Huajie** deduced the mathematical model and assisted in the experiment. Prof. **CAO Xin** revised and modified the manuscript. Ms. **MIAO Wei** contributed to the data for analysis. All authors commented on the manuscript draft and approved the submission.

Competing interests The authors declare no competing interests.

(Production Editor: ZHANG Huangqun)

灵巧机电作动器系统的协调控制策略研究及设计

郝振洋,张绮瑶,陈华杰,曹 鑫,缪 伟

(南京航空航天大学自动化学院,南京 211106,中国)

摘要:为提高灵巧机电作动器(Electromechanical actuator,EMA)系统的频率响应和抗干扰特性,并针对多作动器同步工作时的力纷争问题,提出并设计了基于双闭环负载前馈控制的多输入多输出(Multi input multi output,MIMO)位置差交叉耦合的协调控制策略。该策略利用回差矩阵奇异值法设计满足系统稳定裕度要求的参数范围,并采用灵敏度函数和H_∞范数理论在所得的参数稳定域内设计并确定最优解,使多作动器系统兼具优异的同步性、稳定性和抗干扰性。同时,建立了集成一体化灵巧机电作动器系统的数学模型,根据点-点控制要求,确定并设计了双环控制和负载前馈补偿的控制器,以提高单作动器的频响和抗干扰能力。最后,搭建了270 V高压灵巧机电作动器系统实验平台,进行了频率响应、负载前馈补偿、协调控制实验,验证了位置差交叉耦合控制策略的正确性和参数设计的合理性,使系统达到带宽6 Hz、最大输出力20 000 N、同步误差≤0.1 mm的伺服控制指标,有效解决了力纷争问题。

关键词:灵巧机电作动器;力纷争;协调控制策略;交叉耦合控制;回差矩阵奇异值法;灵敏度H_∞范数控制